Bending sensor based on flexible spin valve

L I Naumova[†], R S Zavornitsyn, M A Milyaev, N G Bebenin, A Y Pavlova, M V Makarova, I K Maksimova, V V Proglyado, A A Zakharov, and V V Ustinov

M.N. Miheev Institute of Metal Physics, Ural Branch, Russian Academy of Sciences, S. Kovalevskoi Street 18, *Ekaterinburg* 620990, *Russia*

(Received 7 June 2022; revised manuscript received 1 August 2022; accepted manuscript online 12 August 2022)

Flexible spin valves were prepared by magnetron sputtering on polyimide substrates. The buffer layer that reduces significantly the effect of the polymer substrate on the spin valve microstructure and magnetoresistive properties was revealed. Bending deformation was applied to the microobjects based on the flexible spin valves in parallel to anisotropy axes. It was revealed that during the bend the magnetoresistance changes due to the joint impact of both the change of the magnetic field projection on the film plane and the change of the magnetic properties of the ferromagnetic layers. The obtained dependences have been used in construction of bending sensor, in which the flexible spin valve microstripes were united into the Wheatstone bridge.

Keywords: spin valve, polymer substrate, magnetostriction, magnetic anisotropy

PACS: 75.80.+q, 68.55.J–, 68.65.Ac, 73.43.Qt **DOI:** 10.1088/1674-1056/ac8923

1. Introduction

Modern electronic devices are being striven to be inexpensive, energy efficient, thin and flexible for use as portable devices such as smart sensors,[1–4] medical devices[5,6] and paper-like displays.[7,8] These devices are usually fabricated on the polymer substrates, such as polyethylene terephthalate (PET), polyetheretherketone (PEEK) and polyimide (PI).

Sputtered on the flexible substrates spin valve nanostructures are the convenient magnetosensitive material. These structures have got a giant magnetoresistive (GMR) effect, an ability to change electrical resistance in the low magnetic fields and high reliability. Spin valve (SV) includes an antiferromagnetic layer and two ferromagnetic (FM) layers separated by a nonmagnetic one.[9] Sputtering in an applied magnetic field forms the uniaxial magnetic anisotropy and sets easy magnetic axis (EA) in SV. The ferromagnetic layer, referred to as a pinned, is coupled by the exchange interaction with the adjacent antiferromagnetic layer. This interaction sets the unidirectional anisotropy with the pinning direction (PD). The pinned layer hysteresis loop shifts from zero field by the exchange bias field (H_{ex}). Another FM layer is called free. The free layer magnetic reversal occurs close to zero field. The free layer hysteresis loop shifts from $H = 0$ by the small field H_j due to the interaction between FM layers. Electrical resistance of SV depends on the angle between the magnetic moments of the FM layers. Both flexible SVs with stable magnetoresistive characteristics and SVs whose properties change during deformation are of interest for the practical use.

In Ref. [10], it was reported about the flexible SV sensors, which exhibit stable GMR effect up to tensile strains of 29% and over 500 bending cycles. In Ref. [11], the sputtered on PI substrate SVs were arranged into Wheatstone bridges and magnetosensitive skins sensors were realized.

The direction of the pinned and free layer magnetic moments and magnetoresistance of SV can be changed by the mechanical stress due to the magnetoelastic Villari effect.[12] In particular, the magnetic permeability changes when a magnetic material is subjected to a mechanical stress and an additional anisotropy appears.[13] The Villari effect is positive or negative, if the additional anisotropy axis is parallel or normal to the deformation vector ($\boldsymbol{u}$).

The strain-induced change of magnetoresistance of the flexible FeMn-based SV due to the orientation of free layer magnetic moment along $\boldsymbol{u}$ was revealed in Ref. [14]. The authors used this property for high sensitive detection of strain direction. It was shown[15,16] that the magnetic anisotropy in a SV can be changed by multiple bending of the nanostructure. In Ref. [17], the dependence of the GMR effect on the tensile and compressive deformation of SV on a PET substrate was studied. In Ref. [18], the flexible spin valves with perpendicular magnetic anisotropy and sensitivity to out-of-plane magnetic field were demonstrated. The authors use Co/Pd-based spin valves with a synthetic antiferromagnet. Few works compare the microstructure, the magnetic and transport properties of nanostructures made on flexible and rigid substrates. In Ref. [19], such a comparison has been made for magnetoimpedance FeNi/Ti-based sensitive elements. In Ref. [20], SV structures were fabricated on the commercial PET foils. It was shown that a high roughness of PET foils is only weakly reflected on SV micro-sensor performance. In Ref. [17], authors compare SVs sputtered on the polymer and SiO_2 substrates, and a reduction of the GMR effect due to the roughness of polymer substrates is investigated.

In the present work, we will study the SV magnetoresis-

[†]Corresponding author. E-mail: naumova@imp.uran.ru

© 2023 Chinese Physical Society and IOP Publishing Ltd

tance variation at the bending taking into account the Villari effect and the change of the nanostructure orientation with the respect to an applied field. We will use the obtained dependencies to design the bending sensor. Special attention is paid to the search of the buffer layer to reduce the effect of a polymer substrate roughness on SV properties.

2. Experiment

SVs of $[Ta(5)/(Ni_{80}Fe_{20})_{60}Cr_{40}(5)]_n/Co_{70}Fe_{20}Ni_{10}(5.5)/Cu(2.6)/Co_{70}Fe_{10}Ni_{20}(4)/Fe_{50}Mn_{50}(15)/Ta(6)$ composition with $n = 2$, 5 and 7 were fabricated by the magnetron sputtering. The nominal thickness of the layers is indicated in nanometers in parentheses. The substrates were prepared as follows. Polyimide film was glued to a glass plate. After sputtering, we separated the PI film with nanostructure from the glass plate. $Co_{70}Fe_{20}Ni_{10}$ alloy with close to zero magnetostriction was used in the free layer. To improve the bending sensitivity of magnetoresistance we used $Co_{70}Fe_{10}Ni_{20}$ alloy with saturation magnetostriction[21,22] $\lambda_s = 1.5 \times 10^{-5}$ in the pinned layer. In our previous article[23] we reported that such SVs exhibit a high magnetoresistance, a low free layer coercivity and a high change of the magnetoresistance under the bending deformation. Investigation of the $[Ta(5)/NiFeCr(5)]_n$ buffer layer roughness was performed by x-ray diffraction and atomic force microscopy (AFM).

Micron sized objects, in particular, microstripes and consisting of two long and two short SV stripes Wheatstone bridge, were made by the optical lithography and ion etching. In the Wheatstone bridge the long and short stripes size were 80 μm×10 mm and 20 μm×2.5 mm, respectively. The width of the microstripes ranged from 20 μm to 100 μm, and the length was 8 mm. Copper contact pads were made by optical lithography and "lift-off" procedure. The size of a flexible sample with a stripe and contact pads on PI substrate was 2 mm×12 mm.

The resistance was measured by dc four-probe method. The magnetoresistance was determined as $\Delta R/R_s = (R(H)–R_s)/R_s$, where $R(H)$ is the resistance in a magnetic field and R_s is the resistance in the saturation field. Evaluation of saturation magnetization was performed by the vibrating-sample magnetometer. All the measurements were performed at room temperature.

We made a holder for bending and uniaxial stretching of the samples. The holder (Fig. 1) consists of plastic channel and non-magnetic screw and nuts. One edge of the sample was fixed to the channel, and the second one makes a translational motion with the nut by the rotation of the screw. The number of the screw rotations (N) clockwise or counter-clockwise controlled the bending and the uniaxial stretching of the sample. The PI substrate thickness (t_s) was 60 μm. The thickness of the sputtered SV nanostructure (t_f) is much smaller than t_s. Thus, we assume that the deformation of the SV film is uniform in volume. Depending on the bending direction, we consider the deformation as linear stretching or compression.

At bending, there is a combination of tensile/compression deformation in the close to the fixation points areas of the sample. To reduce the effect of these areas on the magnetoresistive properties, we fixed the sample in such a way that the area of combined deformation was located under the copper contact pads and $L_{0s} < d$ (Fig. 1).

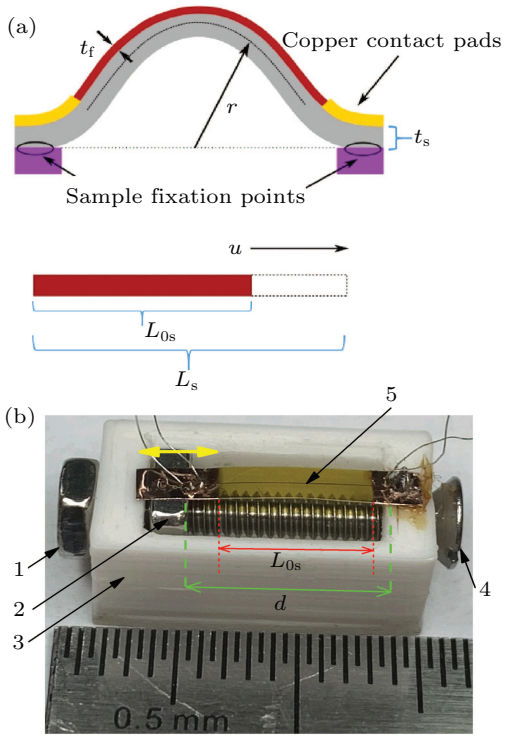


Fig. 1. (a) Schematic representation of a nanostructured film with a thickness t_f on a polymer substrate with a thickness t_s (r is the radius of curvature of the substrate surface, $\boldsymbol{u}$ is the deformation vector, and L_{0s} and L_s are the lengths of the sample in the undeformed and deformed states, respectively). (b) Photo of the holder with a sample. 1, fixation nut; 2, translational square nut; 3, plastic channel; 4, screw; 5, microstripe; d, distance between fixation points; L_{0s}, distance between pads boundaries and length of microstripe to be measured.

We use the deformation vector ($\boldsymbol{u}$), curvature radius of bending (r) and strain (ε) as values characterizing strain for the bending samples. The ε is evaluated from

$$\varepsilon = (t_f + t_s)/2r, \tag{1}$$

as it was done in Ref. [24] for FeGa films grown on the PET substrates.

In the case of uniaxial stretching of the samples without bending the adjacent with SV film part of substrate elongation ($\Delta L_s/L_{0s}$) is used a characterizing strain value

$$\Delta L_s/L_{0s} = (L_s - L_{0s})/L_{0s}, \tag{2}$$

where L_{0s} and L_s are lengths in undeformed and deformed states, respectively. The value of r was estimated by solving

the equation

$$L_{0s} = 2r \arcsin\left(L_{0s} - Nd/2r\right), \tag{3}$$

where N is the number of screw rotation and d is the thread pitch.

3. Results and discussion

3.1. Smoothing the roughness of the PI substrate

To smooth the substrates surface we used the buffer layer of $[Ta(5)/NiFeCr(5)]_n$ with $n = 2$, 5 and 7. Figure 2 shows the typical AFM patterns for PI substrate and for $[Ta/NiFeCr]_5$ sputtered on the PI substrate. The dependence of the average values of roughness on n is shown in Fig. 2(e). The averaging was performed at three random points of the sample surface. The roughness for 1×1 μm is lower than for 5×5 μm. Thus, since the size of the sample decreases, the roughness of the PI substrate should have less impact on magnetoresistive properties of the SV.

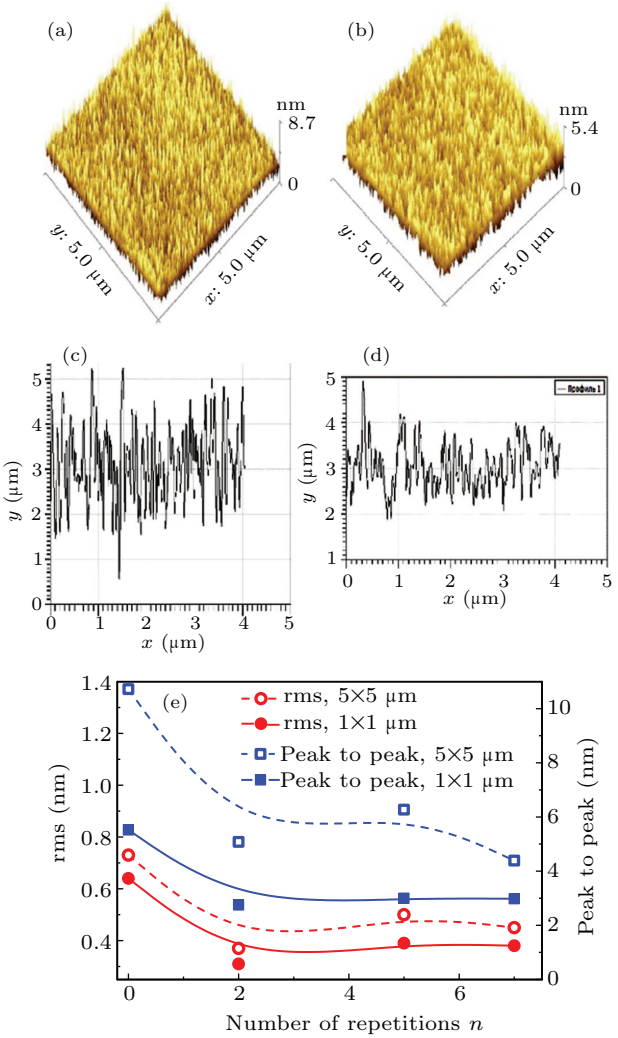


Fig. 2. AFM patterns and the profile for PI substrate (a), (c) and for the coated with $[Ta(5)/NiFeCr(5)]_5$ PI substrate (b), (d) and dependence of the average roughness parameters on n for $[Ta(5)/NiFeCr(5)]_n$ nanostructure sputtered on PI substrate (for the uncoated PI substrate $n = 0$) (e).

X-ray reflectometry was performed for $[Ta(5)/NiFeCr(5)]_5$ nanostructures sputtered on the glass and glass/PI substrates. It was revealed that the rms values for the upper Ta layer were 0.7 nm and 0.6 nm for the samples on glass and PI substrates, respectively. This similarity indicates that the use of $[Ta(5)/NiFeCr(5)]_5$ buffer layer effectively smoothes the roughness of the PI substrate.

XRD investigation of the SV prepared on the PI substrate shows that using PI substrate and $[Ta(5)/NiFeCr(5)]_n$ buffer layer we obtain the microstructure and $\langle 111 \rangle$ texture which are typical for FeMn based SVs.[25]

So, the magnetoresistive properties of the sputtered on PI substrate SV can be improved by two factors: the decrease in the sample size and the increase in the number of repetitions n in $[Ta(5)/NiFeCr(5)]_n$ buffer layer. Resistivity of the buffer layer material (ρ) was estimated for $[Ta(5)/NiFeCr(5)]_5$ sputtered on the glass substrate. The obtained value is sufficiently large ($\rho = 217$ μΩ·cm) therefore, shunting of the current by the buffer layer is insignificant.

3.2. Change of magnetoresistive properties of bent spin valve

3.2.1. Deviation of the non-bent sample from the applied magnetic field

The bending of SVs results in the greatest change in the resistance if $\boldsymbol{u} \parallel \mathrm{PD} \parallel \boldsymbol{H}$.[23] In this case, two factors affect the magnetoresistance: the change of $\boldsymbol{H}$ projection on the film plane and the Villari effect. To study the contribution of these factors separately, we performed the following experiments. We did not bent the SV stripe but turned it in such a way that the field was deviated from the film plane and PD by various angles α. We measured the magnetoresistance curves at different fixed α (Fig. 3).

As the angle α increases, the projection of $\boldsymbol{H}$ on the film plane decreases and the magnetoresistance curves shift to the large fields. Maximal magnetoresistance does not decrease. We do not bend the sample in this experiment and α is the same along the entire SV stripe. Note that in the case of bending the angle α changes from zero in the center to some maximal value ($\alpha_{\max}$) at the edge of the sample (inset of Fig. 3(b)). Thus, the maximal magnetoresistance in $\Delta R/R_s(H)$ curve appears in different field intervals. Thereby the antiparallel mutual orientation of free and pinned layer magnetic moments cannot take place at all points of the stripe. We conclude that this factor leads to decrease of magnetoresistance at bending during both stretching and compression of the SV film.

Figure 3(b) shows the increase of the pinned layer hysteresis loop shift H_{ex} on the angle α if we turn the sample without bending. Let us now consider the bend of the sample and the relationship between the radius r and the angle α between $\boldsymbol{H}$ and the surface of the film. Taking the length of the stripe

L_{0s} as the length of circular arc with radius r, note that the arc-subtending angle is equal to $2\alpha_{max}$ (the inset of Fig. 3(b)). The values of r and α_{max} are related by $L_{0s} = 2\pi r\alpha_{max}/180$. Taking the change of L_{0s} insignificant, $\alpha_{max} \sim 1/r$. Thus, in case of turning the sample the shape of $H_{ex}(\alpha)$ dependence must be close to $H_{ex}(1/r)$ for the bent sample. The difference between $H_{ex}(\alpha)$ and $H_{ex}(1/r)$ dependencies can appear because of the fact that the angle α changes from 0 in the sample center to $\alpha = \alpha_{max}$ and due to the existence of factors other than changing the $\boldsymbol{H}$ projection on the film plane.

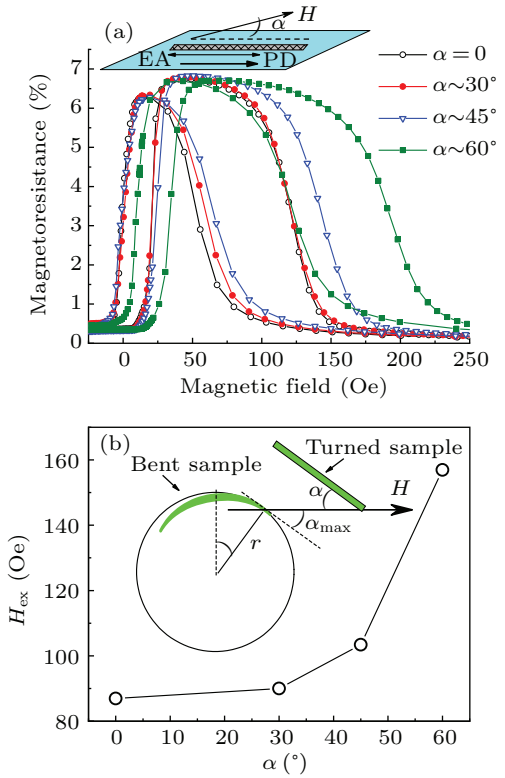


Fig. 3. (a) The magnetoresistance curves for [Ta(5)/NiFeCr(5)]$_5$/$Co_{70}Fe_{20}Ni_{10}$(5.5)/Cu(2.6)/$Co_{70}Fe_{10}Ni_{20}$(4)/FeMn(15)/Ta(6) SV stripe ($w = 80$ μm) (EA ∥ PD) measured at $\boldsymbol{H}$ ∥ PD (empty circles) and at $\boldsymbol{H}$ deviated from the film plane and from the PD by various angles α. (b) Dependence of the field H_{ex} on the angle α. The inset shows schematically the bent and turned samples, where α_{max} is the angle between $\boldsymbol{H}$ and sample plane in the edge of the bent sample.

3.2.2. Uniaxial stretching of the sample without bending

To study the Villari effect contribution we stretched the SV stripe without bending and measured $\Delta R/R_s(H)$ curves in the undeformed state and in the uniaxial stretching state ($\boldsymbol{u}$ ∥ EA ∥ PD). Some of the curves are shown in Fig. 6. High field hysteresis loop refers to the magnetic reversal of the pinned layer. The layer material is $Co_{70}Fe_{10}Ni_{20}$ alloy with $\lambda_s = 1.5 \times 10^{-5}$. When the sample is stretched, the maximal magnetoresistance is increased. In addition, the pinned layer hysteresis loop becomes wider and its slope is decreased. Such changes of the loop are known to be characteristic of the materials with positive magnetostriction.[13] In Ref. [26], the same changes of the hysteresis loop width were observed for CoFeB films grown on flexible PI substrates. Thus, we may conclude that the Villari effect leads to the increase in magnetoresistance of our samples if $\varepsilon > 0$, when $\varepsilon < 0$ the magnetoresistance should certainly decrease.

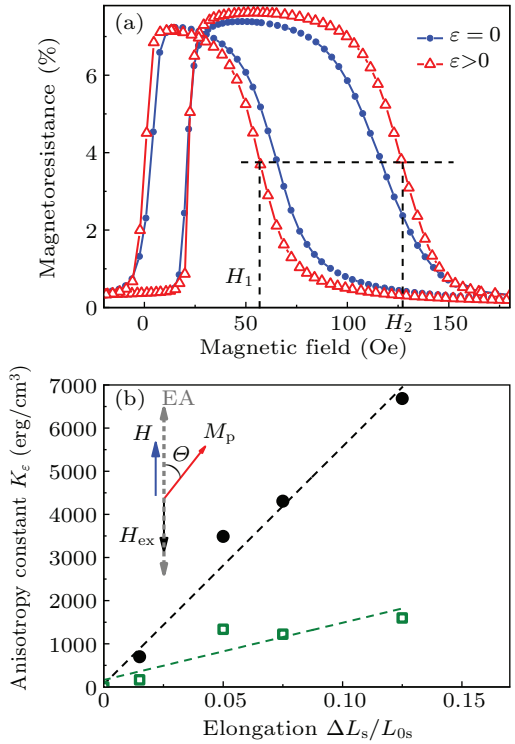


Fig. 4. The magnetoresistance curves for of [Ta(5)/NiFeCr(5)]$_5$/$Co_{70}Fe_{20}Ni_{10}$(5.5)/Cu(2.6)/$Co_{70}Fe_{10}Ni_{20}$(4)/FeMn(15)/Ta(6) SV stripe ($w = 40$ μm) in the undeformed state and under the uniaxial stretching with elongation of 0.125 (a). The dependence of the pinned (solid circles) and free (empty squares) layer magnetoelastic anisotropy constant on elongation (b).

We estimated the stress-induced magnetoelastic anisotropy constants using the Stoner–Wohlfarth model for the pinned layer magnetic reversal. The total free energy F of the pinned layer is given by

$$F = -M_0 H_{ex}\cos\theta - M_0 H\cos(\pi - \theta) + K\sin^2\theta, \qquad (4)$$

where H is the applied magnetic field, H_{ex} is the exchange bias field, θ is the angle between the pinned layer magnetization and EA ∥ PD, and M is the pinned layer saturation magnetization. The anisotropy constant K can be written as sum of two terms

$$K = K_0 + K_\varepsilon, \qquad (5)$$

where K and K_ε are the uniaxial and magnetoelastic anisotropy constants, respectively. Using the minimum of free energy conditions $dF/d\theta = 0$ and $d^2F/d\theta^2 > 0$, we obtained the pinned layer hysteresis loop width

$$H_c = \frac{4K}{M_0}. \qquad (6)$$

Remembering Eq. (6), we can estimate the magnetoelastic anisotropy constant as

$$K_\varepsilon = \frac{1}{4}M_0(H_c^\varepsilon - H_c^0), \qquad (7)$$

where H_c^{ε} and H_c^0 are the pinned layer coercivity in the deformed and undeformed state, respectively. We estimate H_c^{ε} and H_c^0 as a full width at the half height of high field hysteresis loop. For example (Fig. 6(a)),

$$H_c^{\varepsilon} = H_2 - H_1. \tag{8}$$

The pinned layer saturation magnetization $M \approx 1400$ G was evaluated from the magnetic measurements. The dependence of magnetoelastic anisotropy constant on PI substrate elongation is shown in Fig. 4(b).

We used a similar method to estimate the free layer magnetoelastic anisotropy constant. The $K_{\varepsilon}(\Delta L_s/L_{0s})$ dependence for the free layer lies below the dependence for the pinned layer (Fig. 4(b)). The reason is that for the free layer alloy ($Co_{70}Fe_{20}Ni_{10}$) the value of λ_s is close to zero and for the pinned layer alloy ($Co_{70}Fe_{10}Ni_{20}$) $\lambda_s \approx 1.5 \times 10^{-5}$.

It is essential that in our experiment we stretch the lower part of the substrate, glued to the plastic channel and the holder nut, therefore $\Delta L_s/L_{0s}$ refers to only to the lower part of the PI substrate. The deformation of the substrate cannot be uniform because the Young's moduli of the substrate and the SV differ significantly. We may, however, estimate the elastic stress σ in the pinned layer. Figure 4(b) shows that $K_{\varepsilon} \approx 6700$ erg/cm when $\Delta L_s/L_{0s} = 0.125$. It is well-known[27] that

$$K_{\varepsilon} = \frac{3}{2}\lambda_s \sigma. \tag{9}$$

It follows that σ is about 3×10^8 dyn/cm^2. Young's modulus for bulk $Co_{70}Fe_{10}Ni_{20}$ alloy[28] is $E = 1.5 \times 10^{12}$ dyn/cm^2, so the elongation of SV is $\varepsilon = \sigma/E \approx 2 \times 10^{-4}$. This value is indeed much less than $\Delta L_s/L_{0s} = 0.125$.

It is worth noting that Young's modulus of a metallic nanolayer decreases with decreasing film thickness and for the nanolayer it can be significantly less than for a bulk metal.[29,30] Therefore, our calculation gives only rough estimate of ε.

3.2.3. Bending of the sample

Let us return to the consideration of the bent spin valve. The PI substrates with SV stripes were bent step by step with various r by turning the screw in the holder and the magnetoresistance curves were measured at each step. The bending was performed in such a way that tension ($\varepsilon > 0$) or compression ($\varepsilon < 0$) were directed along the SV anisotropy axes. Figure 5 shows some of the measured magnetoresistive curves. The curves before bending and after repeated 40 bending are very close to each other.

The low field parts of the magnetoresistive curves are the same; however, there are some differences in the high field part of these curves. In Ref. [16] the 500-fold bending was found to enhance (or reduce) the magnetoresistance ratio of a spin-valve. We performed the experiment with 40-fold bending accompanied by compression and then 40-fold bending accompanied by stretching. Figure 6 shows the dependencies of maximal magnetoresistance and electrical resistance of the sample in the undeformed state on the number of bend repetitions.

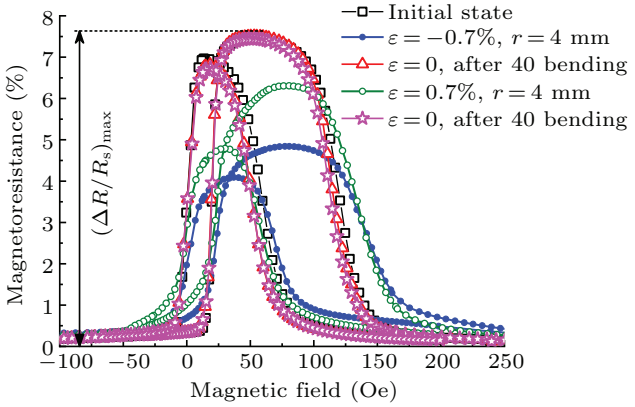


Fig. 5. The magnetoresistance curves for [Ta(5)/NiFeCr(5)]$_5$/$Co_{70}Fe_{20}Ni_{10}$(5.5)/Cu(2.6)/$Co_{70}Fe_{10}Ni_{20}$(4)/FeMn(15)/Ta(6) SV stripe ($w = 100$ μm) measured in the undeformed initial state (squares), in the bending state accompanied by compression ($\varepsilon = -0.7\%$) and by stretching ($\varepsilon = 0.7\%$). In addition, the magnetoresistance curves measured in the undeformed state after 40 bending with $\varepsilon = -0.7\%$ (triangles) and with $\varepsilon = 0.7\%$ (stars) are shown.

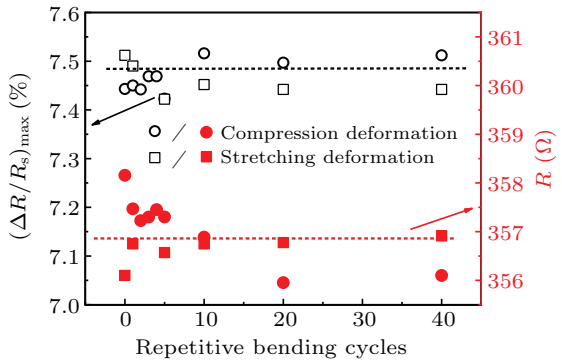


Fig. 6. The maximal magnetoresistance (empty symbols) and electrical resistance (solid symbols) for [Ta(5)/NiFeCr(5)]$_5$/$Co_{70}Fe_{20}Ni_{10}$(5.5)/Cu(2.6)/$Co_{70}Fe_{10}Ni_{20}$(4)/FeMn(15)/Ta(6) SV stripe ($w = 100$ μm) versus number of bend repetitions with $\varepsilon = -0.7\%$ (circles) and $\varepsilon = -0.7\%$ (squares).

Any systematic change of resistance and magnetoresistance at repeated bends of a sample was not revealed.

At bent state, the maximal magnetoresistance is lower than in the undeformed state, $(\Delta R/R_s)_{max}$ being lower for $\varepsilon < 0$ than for $\varepsilon > 0$. Figure 7 shows the dependencies of maximal magnetoresistance and characteristic fields of SV on reverse curvature radius of bend. The values of maximal magnetoresistance $(\Delta R/R_s)_{max}$ were estimated as it is shown for undeformed sample in Fig. 5.

The values of H_j and H_{ex} fields characterize the interaction between free and pinned and between pinned and antiferromagnetic layers. H_j and H_{ex} were estimated as the shift of the middle of the low- and high-field hysteresis loops. Third order polynomial lines fit the experimental data points. The

extremum points for $(\Delta R/R_s)_{max}(1/r)$ and $H_{ex}(1/r)$ fitting lines are shifted to the area corresponding to $\varepsilon > 0$. We suppose that the shift is related with Villari effect. In particular, the change of the field $\boldsymbol{H}$ projection on the film plane leads to the decrease of the magnetoresistance for both $\varepsilon < 0$ and $\varepsilon > 0$ while the Villari effect contribution to the change of magnetoresistance is positive at $\varepsilon > 0$ and negative at $\varepsilon < 0$.

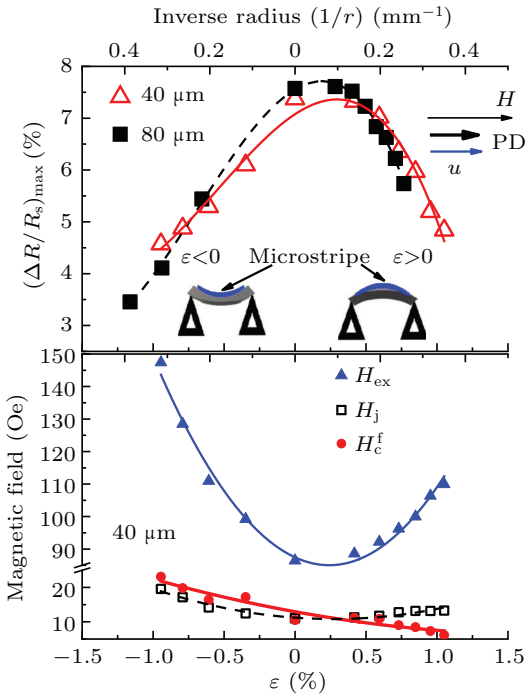


Fig. 7. Dependencies of maximal magnetoresistance, free and pinned layer hysteresis loop shift (H_j and H_{ex}) and free layer coercivity (H_c^f) on the inverse curvature radius of bend for [Ta(5)/NiFeCr(5)]$_5$/$Co_{70}Fe_{20}Ni_{10}$(5.5)/Cu(2.6)/$Co_{70}Fe_{10}Ni_{20}$(4)/FeMn(15)/Ta(6) SV microstripes ($w = 40$ μm and 80 μm).

Strain-induced change in the exchange interaction at ferromagnetic and antiferromagnetic spins and magnetic anisotropy of antiferromagnet exists in $Co_{70}Fe_{10}Ni_{20}$/FeMn. These factors should lead to the alignment of ferromagnetic and antiferromagnetic spins along the PD if $\varepsilon > 0$ and to the disalignment if $\varepsilon < 0$. According to this H_{ex} should increase if $\varepsilon > 0$ and decrease if $\varepsilon < 0$. However, our experiment show another tendency. That is the increase of H_{ex} with the bending accompanied by both compression and stretching of the SV film. Thus, we suppose that in our experiments another factor is more effective. Probably H_j and H_{ex} arise with bending due to the change of projection of $\boldsymbol{H}$ on the film plane, as it is shown in Fig. 3 for H_{ex}. In this case, the change of angle α is equal in bending accompanied by compression or stretching. For $\varepsilon < 0$ the slope of $H_{ex}(\varepsilon)$ is higher than for $\varepsilon > 0$. This difference takes place because the magnetic susceptibility of $Co_{70}Fe_{10}Ni_{20}$ alloy increases at $\varepsilon > 0$ and decreases at $\varepsilon < 0$ because of the positive Villari effect. The same tendency is observed for $H_j(\varepsilon)$ dependence.

The free layer coercivity is characterized by the width of the low field hysteresis loop (H_c). This value increases with bending if $\varepsilon < 0$ and decreases if $\varepsilon > 0$. $Co_{70}Fe_{20}Ni_{10}$ alloy in the free layer has close to zero magnetostriction. Thus $H_c(\varepsilon)$ features are associated with changes in the magnetic properties of the pinned layer. At $\varepsilon > 0$ the local magnetic moments align with SV anisotropy axes, the interaction between ferromagnetic layers increases and the free layer coercivity decreases.[9] At $\varepsilon < 0$ the mismatch of local magnetic moments with anisotropy axes takes place, the interlayer coupling decreases, and free layer coercivity increases.

3.3. Bending sensor

We used the features of $(\Delta R/R_s)_{max}(1/r)$ dependence to create a bending sensor. A Wheatstone bridge circuit connects four SV stripes R1, R2, R3 and R4 making up a rectangle (Fig. 8). The rectangle is made from the SV film in such a way that PD is parallel to the long stripes.

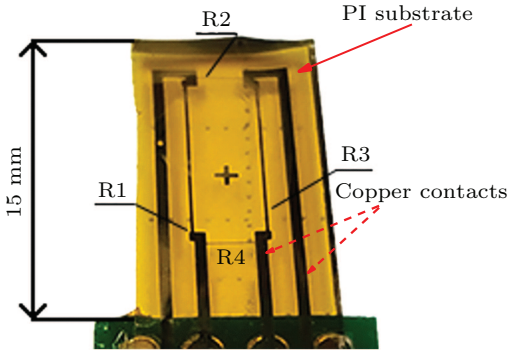


Fig. 8. The photo of the bending sensor with R1, R2, R3 and R4 SV stripes and copper contacts.

At bending the long strips R1 and R3 are subjected to the tensile or compressive deformation. Their resistances reduce. In the short stripes R2 and R4 the field projection decreases when the sensor is bent. As a result, the magnetoresistance curve shifts to the high field region (Fig. 3).

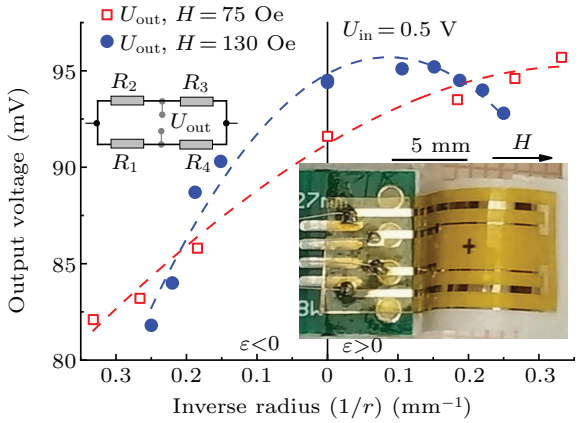


Fig. 9. Dependences of the output voltage of the sensor on inverse radius of bending. Third order polynomial lines fit the data points. The insets show the electric circuit and photo of the sensor in bending state corresponding to stretching of R1 and R3 SV stripes.

Depending on the field in which the measurements are performed, the resistances of the short stripes change or re-

main unchanged, and the sensor works as a half or full Wheastone bridge (Fig. 9).

At bending in the field $H = 75$ Oe the resistance of all stripes decreases. However, under the tension the long stripes resistances R_1 and R_3 decrease more slowly than the short stripes resistances R_2 and R_4. It leads to an increase in the output voltage (U_{out}). For $H = 130$ Oe the short stripes resistances do not change because this field corresponds to a plateau on the magnetoresistance curve. Thus, a decrease in R_1 and R_3 leads to a decrease in U_{out} when the bending is accompanied by both tension and compression of the nanostructure.

4. Conclusion

It was revealed that the buffer layer of $[\text{Ta}(5)/(\text{Ni}_{80}\text{Fe}_{20})_{60}\text{Cr}_{40}(5)]_n$ composition with $n = 5$–7 repetitions reduces significantly the effect of the polymer substrate roughness on the magnetoresistance and the interlayer interaction in the spin valve. Using the flexible polyimide film as the substrate and $[\text{Ta}(5)/\text{NiFeCr}(5)]_n$ as a buffer layer the spin valve with perfect $\langle 111 \rangle$ texture and the typical for FeMn-based spin valves microstructure were obtained.

It was shown that the reduction in size of the sample to several tens of microns is the effective method to improve the magnetoresistive properties of the sputtered on polymer substrate spin valve.

The magnetoelastic anisotropy constants and the elongation of the spin valve film sputtered on PI substrate have been estimated by using the magnetoresistive measurements.

If the deformation vector is parallel to pinning direction of spin valve, the change of magnetoresistance during bending is the result of joint impact of both: change of the magnetic field projection on the film plane and the change of magnetic properties of layers due to the Villari effect.

The revealed buffer layer and researched magnetoresistive properties of the flexible spin valve were realized in the bending sensor. We demonstrated its performance in the different magnetic fields.

Acknowledgements

This study was performed within the framework of State Assignment from the Ministry of Education and Science of Russian Federation (topic Spin, No. 122021000036-3 and topic Magnet, No. 122021000034-9) and partially supported by the Russian Foundation for Basic Research (project No. 20-42-660018).

References

[1] Gaspar J, Fonseca H, Paz E, Martins M, Valadeiro J, Cardoso S, Ferreira R and Freitas P P 2017 *IEEE Trans. Magn.* **53** 1

[2] Wang Z, Wang X, Li M, Gao Y, Hu Z, Nan T, Liang X, Chen H, Yang J, Cash S and Sun N X 2016 *Adv. Mater.* **28** 9370

[3] Makarov D, Melzer M, Karnaushenko D and Schmid O 2016 *Appl. Phys. Rev.* **3** 011101

[4] Sheng P, Wang B and Li R 2018 *J. Semiconduct.* **39** 011006

[5] Cardoso S, Leitao D C, Dias T M, Valadeiro J, Silva M D, Chicharo A, Silverio V, Gaspar J and Freitas P P 2017 *J. Phys. D* **50** 213001

[6] Delipinar T, Shafique A, Sepehri Gohar M and Kaya Yapic M 2021 *ACS Omega* **6** 8744

[7] Rogers J A, Bao Z, Baldwin K, Dodabalapur A, Crone B, Raju V R, Kuck V, Katz H, Amundson K, Ewing J and Drzaic 2001 *Proc. Natl. Acad. Sci. USA* **98** 4835

[8] Zhou L, Wang A, Wu S C, Sun J, Park S and Jackson T 2006 *Appl. Phys. Lett.* **88** 083502

[9] Kools J 1996 *IEEE Trans. Magn.* **32** 3165

[10] Melzer M, Lin G, Makarov D and Schmidt O G 2012 *Adv. Mater.* **24** 6468

[11] Bermúdez G, Karnaushenko D D, Karnaushenko D, Lebanov A, Bischoff L, Kaltenbrunner M, Fassbender J, Schmidt O G and Makarov D 2018 *Science Advances* **4** 2623

[12] Ota S, Ando A and Chiba D 2018 *Nat. Electron.* **1** 124

[13] Cullity B and Graham C D 2008 *Introduction to Magnetic Materials*, Second Edition (IEEE Press) p. 258 ISBN 978-0-471-47741-9

[14] Matsumoto H, Ota S, Ando A and Chiba D 2019 *Appl. Phys. Lett.* **114** 132401

[15] Kwon J H, Kwak W Y and Ki Cho B 2018 *Sci. Rep.* **8** 15765

[16] Kwon J H, Kwak W Y, Choi H Y, Kim G H and Cho B K 2015 *J. Appl. Phys.* **117** 17

[17] Guo Q, Xu X G, Zhang Q Q, Liu Q, Wu Y J, Zhou Z Q, Zhu W M, Wu Y, Miaoa J and Jiang Y 2016 *RSC Advances* **6** 88090

[18] Makushko P, Mata E, Bermúdez G, Hassan M, Laureti S, Rinaldi C, Fagiani F, Barucca G, Schmidt N, Zabila Y, Kosub T, Illing R, Volkov O, Vladymyrskyi I, Fassbender J, Albrecht M, Varvaro G and Makarov 2021 *Adv. Funct. Mater.* **31** 2101089

[19] Kurlyandskaya G V, Fernández E, Svalov A, Burgoa Beitia A, García-Arribas A and Larra naga A 2016 *J. Magnet. Magnet. Mater.* **415** 91–96

[20] Ferreira M, Mouro J, Silva M, Silva A, Cardoso S and Leitao D 2021 *J. Magnet. Magnet. Mater.* **538** 168153

[21] Zhang Y, Zhang M, Li D, Zuo T, Zhou K, Gao M C, Sun B and Shen T 2019 *Metals* **9** 382

[22] Meguro K, Hirano S, Jimbo M, Tsunashima S and Uchiyama S 1995 *J. Magnet. Magnet. Mater.* **140–144** 601–602

[23] Naumova L I, Chernyshova T A, Zavornitsyn R S, Milyaev M A, Maksimova I K, Proglyado V V, Zakharov A A and Ustinov V V 2021 *Phys. Metals Metallography* **122** 1066

[24] Dai G, Zhan O, Liu Y, Yang H, Zhang X, Chen B, and Li R W 2012 *Appl. Phys. Lett.* **100** 122407

[25] Kamiguchi Y, Saito K, Iwasaki H, Sahash M, Ouse M and Nakamura S 1996 *J. Appl. Phys.* **79** 6399

[26] Zhang H, Li Y Y, Yang M Y, Zhang B, Yang G, Wang S G and Wang K Y 2015 *Chin. Phys. B* **24** 077501

[27] Kittel C 1949 *Rev. Mod. Phys.* **21** 541

[28] Jen S U, Chiang H P, Chung C M and Kao M N 2001 *J. Magnet. Magnet. Mater.* **236** 312

[29] Kim Y Y 2017 *Materials* **10** 806

[30] Zhu F, Xie Z and Zhang Z 2018 *AIP Advances* **8** 035321